Mem. S.A.It. Suppl. Vol. 4, 17


**Memorie** della
**Supplementi**


# An accurate numerical approach for the kinematic dynamo problem

A. Bonanno

INAF- Osservatorio Astrofisico di Catania, Via S.Sofia 78, I - 95123 e-mail: alfio@ct.astro.it

**Abstract.** A high-precision code which solves the spherical kinematic dynamo problem in the case of high magnetic Reynolds number is presented. In particular the solar dynamo case is discussed for a multi-cell meridional flow and for a helioseismically derived solar rotation law. Particular attention is given to the parity problem selection, and to the detection of multi-critical solutions.

**Key words.** Dynamo theory - Spectral Methods

## 1. Introduction

Kinematic dynamo models are important tools in turbulent MHD in astrophysics. In recent years there has been a lot of work in this direction mainly because helioseismology provide us with an accurate detection of the rotation law inside a star.

In particular it has been realized that if the eddy diffusivity is small enough $\eta_{\rm T}$, the meridional flow $u_{\rm m}$ plays an important role in deforming the toroidal magnetic field belts (Wang et al. 1991; Choudhuri et al. 1995) in the kinematic solar dynamo problem. In this model the rotation law can be considered as given (known from helioseismology), and one is in general free to vary the location of the turbulent layer, where the magnetic field amplification occurs.

In particular, for $\eta_{\rm T} = 10^{11}{\rm cm}^2/{\rm s}$ , as is known from the sunspot decay, the magnetic Reynolds number ${\rm Rm} = u_{\rm m}R_\odot/\eta_{\rm T}$ reaches values of the order of $10^3$ for a flow of 10 m/s. As a consequence, depending on the localization of the dynamo wave, a dramatic modification of both magnetic field configurations and cycle period is expected. This possibility has recently been a subject of intense numerical investigation (Dikpati & Charbonneau 1999; Küker et al. 2001, Bonanno et al. 2002), where it has been shown that solutions with high magnetic Reynolds number provide correct cycle period, butterfly diagrams, magnetic phase relations and sign of current helicity, by means of a *positive* $\alpha$-effect in the north hemisphere.

It is here presented an accurate numerical eigenvalue method which can be very useful in solving the advection-dominated spherical kinematic dynamo model. In particular it is studied how the presence of the flow and the location of the turbulent layer affect the parity mode selection and the cycle period. Thanks to the numerical accuracy, it is shown that, for high magnetic Reynolds numbers of the flow, quadrupolar field configurations are more easily excited than the dipolar ones if there is no $\alpha$-effect below $r/R_\odot \approx 0.8$.

Moreover, it is also discussed an application of this method to the problem of finding multi-critical solution to dynamo excitation condition.

## 2. The kinematic dynamo problem

The kinematic dynamo problem is that of determining whether a flow **u** moving in a body of volume $V$ can amplify or maintain a magnetic field **B** without the presence of external sources. The mathematical problem is represented by the pre-Maxwell equations

$$\mathrm{rot}\,\boldsymbol{E} = -\frac{\partial \boldsymbol{B}}{\partial t} \quad \mathrm{rot}\,\boldsymbol{B} = \mu \boldsymbol{j} \quad \mathrm{div}\,\boldsymbol{B} = 0 \tag{1}$$

and Ohm's law

$$\boldsymbol{j} = \sigma(\boldsymbol{E} + \boldsymbol{u} \times \boldsymbol{B}) \tag{2}$$

where $\mu$ and $\sigma$ are the permeability and the conductivity of the fluid (for the moment assumed constant, and $\eta_{\mathrm{T}} = 1/\mu\sigma$ is the turbulent diffusivity). As it is well known, no fields obeying (1) and (2) exist if $\boldsymbol{B}$ is axisymmetric. The situation radically changes in the presence of turbulence for which the fluid velocity $\boldsymbol{u}$ and therefore the field $\boldsymbol{B}$ can be divided into mean parts $\langle \boldsymbol{u} \rangle$, $\langle \boldsymbol{B} \rangle$ and fluctuating parts $\boldsymbol{u'}$, $\boldsymbol{B'}$ so that

$$\boldsymbol{u} = \langle \boldsymbol{u} \rangle + \boldsymbol{u'} \quad \boldsymbol{B} = \langle \boldsymbol{B} \rangle + \boldsymbol{B'} \tag{3}$$

Since Maxwell equations are linear these holds as before with the brackets added. Ohm's law, however, reads

$$\langle \boldsymbol{j} \rangle = \sigma(\langle \boldsymbol{E} \rangle + \langle \boldsymbol{u} \rangle \times \langle \boldsymbol{B} \rangle + \boldsymbol{\mathcal{E}}) \tag{4}$$

where

$$\boldsymbol{\mathcal{E}} \equiv \langle \boldsymbol{u'} \times \boldsymbol{B'} \rangle \tag{5}$$

is referred as "mean electromotive force". This term can be calculated by examining the induction on the microscopic scale and it can be exhibited as a linear functional of the mean magnetic field. In the following we shall discuss the simplest choice, where the linear combination reduces to only one term, $\alpha\langle B_j \rangle$, the so called $\alpha$-effect.

## 3. Basic equations

In the following the dynamo equations are given for axial symmetry and the inclusion of the induction by meridional circulation. The induction equation also derivable from (1) and (2) may be written in the form

$$\begin{aligned} \frac{\partial \boldsymbol{B}}{\partial t} &= \mathrm{rot}(\boldsymbol{u} \times \boldsymbol{B} + \alpha \boldsymbol{B}) \\ &- \mathrm{rot}\,(\sqrt{\eta_{\mathrm{T}}}\,(\mathrm{rot}\,\sqrt{\eta_{\mathrm{T}}}\boldsymbol{B})) \end{aligned} \tag{6}$$

which includes the diamagnetism due to non-uniform turbulence. In this case (Kitchatinov& Rüdiger, 1992) the diffusive part of the mean turbulent electromotive force reads $-\eta_{\mathrm{T}}\mathrm{rot}\boldsymbol{B} - \nabla\eta_{\mathrm{T}} \times \boldsymbol{B}/2 = -\sqrt{\eta_{\mathrm{T}}}\mathrm{rot}\sqrt{\eta_{\mathrm{T}}}\boldsymbol{B}$ where the second term is due to the turbulent diamagnetism. When strong gradients of turbulence intensity are present, this term will dominate the transport of the mean magnetic fields.

Axisymmetry implies that the magnetic field **B** and the mean flow field **U** in spherical coordinates are given by

$$\mathbf{B} = B_\phi(r,\theta,\phi)\hat{\mathbf{e}}_\phi + \nabla \times [A(r,\theta,t)\hat{\mathbf{e}}_\phi] \tag{7}$$

$$\mathbf{U} = \mathbf{u}(r,\theta) + r\sin\theta\Omega(r,\theta)\hat{\mathbf{e}}_\phi \tag{8}$$

where $B_\phi(r,\theta,\phi)$ and $[A(r,\theta,t)\hat{\mathbf{e}}_\phi]$ corresponds to the toroidal and poloidal components of the magnetic field, and the meridional circulation $\mathbf{u}(r,\theta)$ and differential rotation $\Omega(r,\theta)$ to the poloidal and toroidal parts of the full flow field **U**.

The induction equation reads:

$$\begin{aligned} &\frac{\partial A}{\partial t} + \frac{1}{s}(\mathbf{u}\cdot\nabla)(sA) = \alpha B + \\ &\frac{\sqrt{\eta_{\mathrm{T}}}}{r}\frac{\partial}{\partial r}\sqrt{\eta_{\mathrm{T}}}\frac{\partial Ar}{\partial r} + \frac{\eta_{\mathrm{T}}}{r^2}\frac{\partial}{\partial\theta}\frac{1}{s}\frac{\partial As}{\partial\theta} \\ &\frac{\partial B}{\partial t} + s\rho(\mathbf{u}\cdot\nabla)\frac{B}{s\rho} = \end{aligned} \tag{9}$$

$$\begin{aligned} &\left(\frac{\partial\Omega}{\partial r}\frac{A\sin\theta}{\partial\theta} - \frac{1}{r}\frac{\partial\Omega}{\partial\theta}\frac{\partial sA}{\partial r}\right) + \\ &\frac{1}{r}\frac{\partial}{\partial r}\sqrt{\eta_{\mathrm{T}}}\frac{\partial}{\partial r}(r\sqrt{\eta_{\mathrm{T}}}B) + \frac{\eta_{\mathrm{T}}}{r^2}\frac{\partial}{\partial\theta}\frac{1}{s}\frac{\partial Bs}{\partial\theta} - \\ &\frac{1}{r}\frac{\partial}{\partial r}\left(\alpha\frac{\partial Ar}{\partial r}\right) - \frac{\partial}{\partial\theta}\left(\frac{\alpha}{\sin\theta}\frac{\partial A\sin\theta}{\partial\theta}\right) \end{aligned} \tag{10}$$

where $s = r\sin\theta$. The meridional circulation is derived from a linear combination of stream functions, by introducing a series expansion in Legendre polynomials $P_n^{(1)}$ as described in Rüdiger (1989):

$$\psi(r,\theta) = \sum_{n,4} \Psi_n(r) P_n^{(1)} \sin\theta \tag{11}$$

so that the condition $\mathrm{div}\,\rho\boldsymbol{u} = 0$ is automatically fulfilled. In particular

$$\hat{u}_r = \frac{1}{r^2\hat{\rho}\sin\theta}\frac{\partial\psi}{\partial\theta} = \sum_{2,4}\frac{1}{\hat{\rho}r^2}\, n(n+1)\Psi_n P_n \tag{12}$$

$$\hat{u}_\theta = -\frac{1}{r\hat{\rho}\sin\theta}\,\frac{\partial\psi}{\partial r} = -\sum_{2,4}\frac{1}{\hat{\rho}r}\,\frac{d\Psi_n}{dr}P_n^{(1)}. \tag{13}$$

A two-cell meridional circulation is thus described by

$$u_r = \frac{5}{2\rho r^2}(35\cos^4\theta - 30\cos^2\theta + 3)\Psi_4$$

$$u_\theta = -\frac{(70\cos^3\theta - 30\cos\theta)\sin\theta}{4\rho r}\frac{d\Psi_4}{dr},$$

where a positive $\Psi_4$ describes a cell circulating clockwise in the northern hemisphere, i.e. the flow is polewards at the bottom of the convection zone and equatorwards at the surface. In order to keep the flow inside the convection zone, the function $\Psi_n$ must be zero at the surface and at the bottom of the convection zone. An example of stream function for a two-cell meridional flow is shown is figure.

The rotation law for the solar dynamo can be considered as given by the helioseismic observations, in particular the analytical model of Dikpati & Charbonneau (1999) which is characterized by the existence of a steep subrotation profile in the polar region with a thickness of about 0.05 solar radii is used. The radial profile of $\eta_\mathrm{T}$ is defined as

$$\eta_\mathrm{T} = \eta_c + \frac{1}{2}(\eta_t - \eta_c)(1 + \mathrm{erf}(40(x - 0.7))), \tag{14}$$

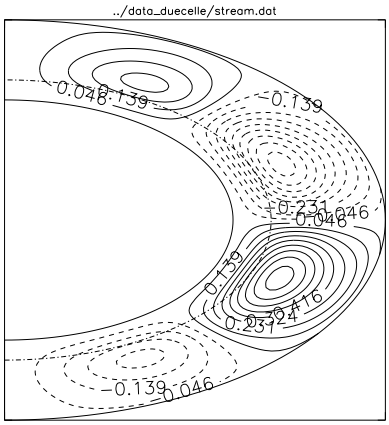


**Fig. 1.** Isocontour lines of the the stream function $\psi$ of the meridional circulation used in the model computations. Solid line represent a positive stream function and dashed represent negative $\psi$

where $x = r/R_\odot$ is the fractional radius, *erf* denotes the error function, $\eta_t$ is the eddy diffusivity, and $\eta_c$ the magnetic diffusivity beneath the convection zone. The factor 40 defines the thickness of the transition region to be $0.05R_\odot$, and we have adopted both $\eta_c/\eta_t = 0.1$ and $\eta_c/\eta_t = 0.02$.

The SOCA theory of Lorentz force-driven turbulence in a stratified rotating plasma also leads to negative current helicity and positive $\alpha$-effect for the northern hemisphere.

The $\alpha$-effect is always antisymmetric with respect to the equator, so that

$$\alpha = \alpha_0\cos\theta\Big(1 + \mathrm{erf}(\frac{x - x_\alpha}{d})\Big)\Big(1 - \mathrm{erf}(\frac{x - x_\beta}{d})\Big)/4, \tag{15}$$

where $\alpha_0$ is the amplitude of the $\alpha$-effect and $x_\alpha$, $x_\beta$ and $d$ define the location and the thickness of the turbulent layer, respectively. Differently from the overshoot dynamo $\alpha_0$ is *not* assumed to change its sign in the bulk of the convection zone or in the overshoot layer. In Fig. 2 the eddy diffusivity profile and the $\alpha$ profile are shown for $x_\alpha = 0.9$, $x_\beta = 1$ and

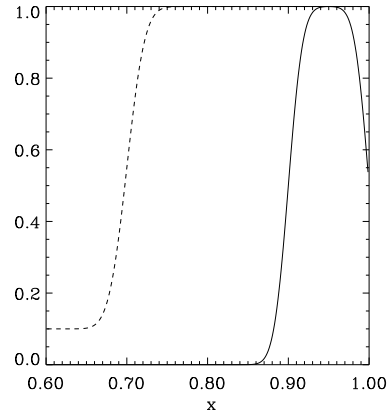


**Fig. 2.** The $\alpha$-effect normalized function in the bulk of the convection zone (solid line) and the profile of the eddy diffusivity (dashed line).

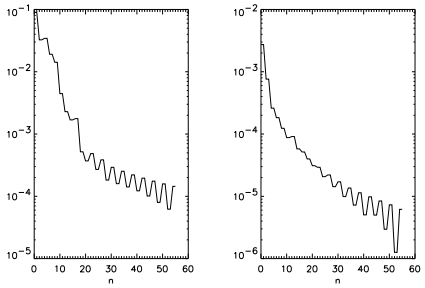


**Fig. 3.** Truncation dependence of a typical high-Reynolds number solution. The quantities $\max_x\{b_n\}$ and $\max_x\{a_n\}$ as a function of $n$ are shown, in the left and in the right panel, respectively.

$d = 0.05$ which correspond to an $\alpha$-effect located at the top of the convection zone.

## 4. Mathematics and numerics

In order to investigate the properties of the solar dynamo with such a low eddy diffusivity the linear dynamo Eq. (6) is solved with a finite-difference scheme for the radial dependence and a polynomial expansion for the angular dependence. In particular, the following expansions for the field is used:

$$\hat{A}(x,\theta) = e^{\lambda t} \sum_n a_n(x)\, P_n^{(1)}(\cos\theta), \tag{16}$$

$$\hat{B}(x,\theta) = e^{\lambda t} \sum_m b_m(x)\, P_m^{(1)}(\cos\theta), \tag{17}$$

where $\lambda$ is the (complex) eigenvalue, $n = 1, 3, 5, \ldots$ and $m = 2, 4, 6, \ldots$ for antisymmetric modes, and $n \leftrightarrow m$ for symmetric modes. Vacuum boundary conditions at the surface are then translated into

$$\frac{da_n}{dx} + (n+1)\, a_n = b_m = 0. \tag{18}$$

In the interior at $x = x_{\rm i} = 0.6$ we have instead set

$$x\frac{db_m}{dx} + b_m = a_n = 0, \tag{19}$$

which imply perfect conductor boundary conditions for the field.

By substituting (16) and (17) in (6) one obtains a set of infinite o.d.e. that can be conveniently truncated in $n$ when the desired accuracy is achieved. The system is in fact solved by means of a second order accuracy finite difference scheme and the basic computational task is thus to numerically compute eigenvalues and eigenvectors of a block-band diagonal real matrix of dimension $M \times n$, $M$ being the number of mesh points and $n$ the number of harmonics,

$$M(\alpha)v = \lambda v \tag{20}$$

and $v$ is in general a complex eigenvector.

This basic algorithm is embedded in a bisection procedure in order to determine the critical $\alpha$-value needed to find a purely oscillatory solution, for which

$$\Re e(\lambda) = 0 \tag{21}$$

Numerically a zero is accepted when the dimensionless quantity $\Re e(\lambda) R_\odot^2/\eta_{\rm T}$ is no greater than $10^{-3}$ in the following calculations. More accuracy requires usually a more refined spatial grid.

The accuracy of the code has been tested in cases where the eigenvalues and eigenfunctions are known (decay modes with $\alpha = 0$

and simple analytic solutions with constant $\alpha$). Furthermore, most of the solutions discussed in the literature (no flow) have been reproduced and good agreement was found. In fact one has rapid convergence in $n$ for simple (no-flow) $\alpha\Omega$-dynamo, but when the flow is present, the number of harmonics needed in order to get convergence generally increases with the Reynolds number. In this case it is necessary to truncate the series (18-19) when the maximum value over $x$ of the $n$-th harmonic drops by roughly three orders of magnitude, as shown in Fig. 3.

## 5. Numerical results

### 5.1. single cell flow

The results can be summarized in Table I where critical $\alpha$-values (cm/s) and periods (yrs) for a very thin $\alpha$-layer located between $x_\alpha = 0.7$ and $x_\beta = 0.75$ for various values of the flow (m/s), for both antisymmetric and symmetric field configurations are shown. In the last line the same $\alpha$-layer is located between $x_\alpha = 0.95$ and $x_\beta = 1$ and the solution is clearly of the symmetric type. The effect of the flow is dramatic in determining both the parity and the field topology of the solution. The butterfly diagram is also correct as shown in Fig. 1. where the alpha-effect was at the bottom for a very thin layer, with $u_\mathrm{m} = 12$ m/s at $t = 0$ and $x_\alpha = 0.7$, $x_\beta = 0.75$

### 5.2. 2-cell flow

It is also interesting to see that the solution for a two-cell flow. The topology of the meridional flow is shown in figure (8). In this case we have a strong equatorwards flow at lower latitudes, and the resulting butterfly diagram is depicted in figure (9). The basic input parameters are $u_m = 3.6m/sec$, $\alpha$ is positive in the all convection zone, and the period is 22.5 years.

### 5.3. multi-critical dynamo solutions

A multi-critical dynamo is a dynamo which can be excited for different values of the turbulent helicity. Mathematically this is equivalent to find multiple values of $\alpha_0$ for which the criticality condition (21) holds. This is an important application because many astrophysical situations can be discussed in this framework (see the FK-Comae Flip-Flop phenomenon).

Let us now consider a simple rotation law $\Omega \propto r$ in a full convective star, *i.e.* the $\alpha$-effect extends all over the star, and define the dynamo numbers $C_\alpha = \alpha R/\eta_\mathrm{T}$, and $C_\Omega = R^2\Omega'/\eta_\mathrm{T}$.

Then the locus of all possibles solution can be described by the plot in figure (10) where the triangle represent oscillating solu-

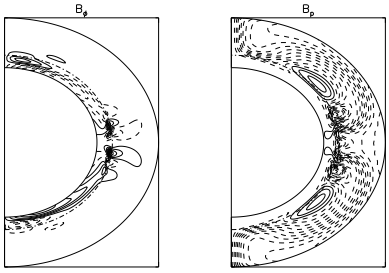


**Fig. 4.** Thin Alpha-effect at the bottom: Toroidal (left) and poloidal (right) antisymmetric (dipolar) field configuration for $\alpha$= 4.36 cm/s, $u_\mathrm{m} = 3$ m/s at $t = 0$ and $x_\alpha = 0.7$, $x_\beta = 0.75$.

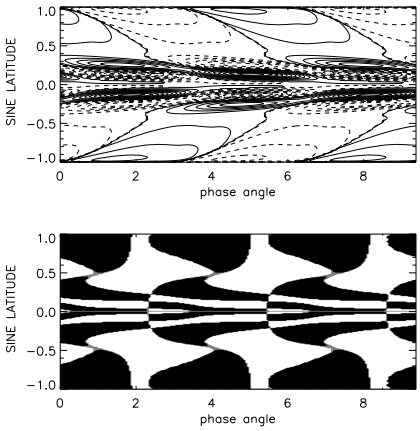


**Fig. 5.** Butterfly diagram and $B_r B_\phi$ sign (negative < 0) for the model presented in Fig. 4. The cycle period is 74 years.

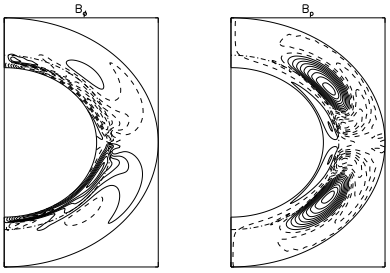


**Fig. 6.** Alpha-effect at the bottom for a very thin layer: toroidal (left) and poloidal (right) antisymmetric (dipolar) field configuration for $\alpha$= 16.61 cm/s, $u_{\rm m}$ = 12 m/s at $t$ = 0 and $x_\alpha$ = 0.7, $x_\beta$ = 0.75 .

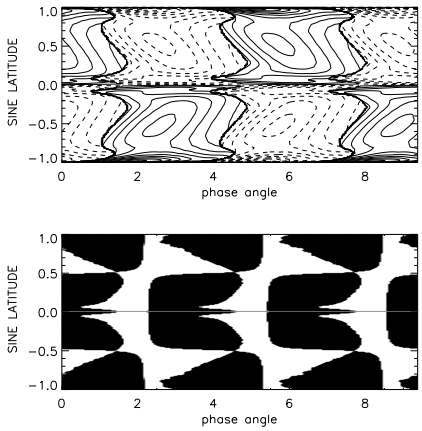


**Fig. 7.** Butterfly diagram and $B_r B_\phi$ sign (negative < 0) for the model presented in Fig. 6. The cycle period is 23 years.

tions while the squares and crossed-squares represent static solutions. There are thus two branches of possible solutions for $C_\Omega$ less of $\approx$ 185. It is also interesting to note that the point $F$ shows the coexistence of a static and oscillating solution for the same value of $C_\alpha$.

Although the fate of this solution can only be discussed within a non-linear calculation, it is mandatory to understand the possibility of the occurrence of such solutions already at the linear level, in order to understand the non-linear behavior.

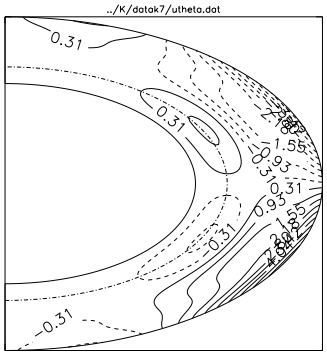


**Fig. 8.** Isocontour lines of the $u_\theta$ component of the meridional flow. Dashed line is negative $u_\theta$

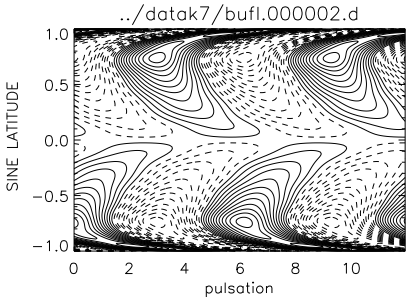


**Fig. 9.** Butterfly diagram for the two-cell discussed in the text

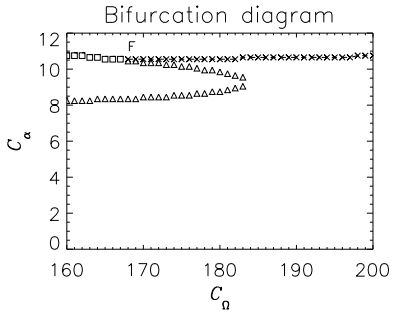


**Fig. 10.** "bifurcation" diagram for static and oscillating solutions (see the text).

## 6. Conclusions

A numerical eigenvalue code has been developed in order to solve the kinematic dynamo models for very high Reynolds numbers.

| $u_m$ | $\alpha_A$ | $P_A$ | $\alpha_S$ | $P_S$ |
|---|---|---|---|---|
| 1 | **0.43** | $\infty$ | 1.14 | 90.8 |
| 2 | **1.37** | $\infty$ | 1.83 | $\infty$ |
| 3 | **4.36** | 74 | 4.94 | 64 |
| 5 | **7.53** | 38 | 8.46 | 35 |
| 7 | **9.22** | 34 | 9.65 | 33 |
| 12 | **16.61** | 23 | 16.77 | 23 |
| 2 | 87 | $\infty$ | 50 | 283 |
| 20 | 43 | 94 | 40 | 68 |

**Table 1.** Critical $\alpha$-values (cm/s) and periods (yrs) for a very thin $\alpha$-layer located between $x_\alpha = 0.7$ and $x_\beta = 0.75$ for various values of the flow (m/s), for both antisymmetric and symmetric field configurations.

An eddy diffusivity of $10^{11}$ cm$^2$/s provides us with a value consistent with the sunspot decay. With such a small value the magnetic Reynolds number for a meridional flow of (say) 10 m/s reaches values of order of $10^3$, so that the dynamo can really be called advection-dominated. The result of this computation shows that the meridional flow advects the field equatorwards producing a butterfly diagram of the observed type, which would not occur with i) a positive $\alpha$-effect (in the northern hemisphere), ii) the standard rotation law known from helioseismology and iii) no meridional flow (Choudhuri et al. 1995; Dikpati & Charbonneau 1999; Küker et al. 2001). It was shown the important role of the global topology of the meridional circulation in determining the correct butterfly diagram. A determination of multi-critical dynamo solutions is also very clearly detected with this method. It is also possible to extend the approach in the case of non-axisymmetric fields and this project is currently under investigation.

## References

Bonanno, A., Elsner D., RüdigerG., Belvedere G., A&A, 690, 673

Choudhuri, A.R., Schüssler, M., & Dikpati, M. 1995, A&A, 303, L29

Dikpati, M., & Charbonneau, P. 1999, *Astrophys. J.* **,**, 518,508

Dikpati, M., & Gilman, P.A. 2001, *Astrophys. J.* **,**, 559,428

Küker, M., Rüdiger, G., & Schultz, M. 2001, A&A, 374, 301

Rüdiger, G. 1989, Differential Rotation and Stellar Convection: Sun and Solar-type stars. (Gordon & Breach Science Publishers, New York)

Wang, Y.-M., Sheeley, N.R., Jr., & Nash, A.G. 1991, *Astrophys. J.* **,** 383,431